



Full Paper

Angela Kirsti A.Lim¹, Gene Q.Blantocas^{2*}, Fahad Al-Mufadi³

¹National Institute of Physics, College of Science, University of the Philippines, Diliman, Quezon City, (PHILIPPINES)

²College of Architecture, Design and Planning, Qassim University, Buraydah, Al-Qassim, (KINGDOM OF SAUDI ARABIA)

³College of Engineering, Qassim University, Buraydah, Al-Qassim, (KINGDOM OF SAUDI ARABIA)

E-mail : gqblantocas@gmail.com

Received: December 08, 2013

Accepted: February 15, 2014

*Corresponding author's
Name & Address

Gene Q.Blantocas

College of Architecture, Design and Planning, Qassim University, Buraydah, Al-Qassim, (KINGDOM OF SAUDI ARABIA)

E-mail : gqblantocas@gmail.com

Texturing the surface of CR-39 ophthalmic lenses by low energy hydrogen ion shower: Profiling the physicochemical and optical properties of the textured surface vis-à-vis ion shower characteristics

Abstract

Hydrogen ion showers (H_n^+) of current densities 50 to 400 mA/m² were irradiated on AlyllDiglycol Carbonate (CR-39) ophthalmic lenses. The substrate lenses measured 6×6×2 mm³ and were fabricated through hot deformation polymerization process. Irradiation time was fixed at 15 minutes per sample. The study aimed to correlate H_n^+ ion beam characteristics to the physicochemical and optical changes of the treated lenses. Beam current densities were measured using a cast steel mass spectrometer and emittance contours at 90 % beam fraction were measured using a single-slit multi-detector emittance meter. Unnormalized emittances ranged from 180 to 310 mm-mrad for 1 to 5 mA discharges. Low energy beams (< 1keV) with elliptic emittance contour shaving H^+/H_2^+ ratio > 8 produced a ubiquitous feature of tapered nanostructures on the surfaces. AFM histograms showed that average substrate surface roughness decreased from 30.91 nm (pristine sample) to 12.94 nm (treated samples) when low energy beams were used, but increased to 20.33 for high energy beams. Lens hydrophobicity improved with contact angles increasing from 61.23° (pristine) to 122.64° (treated). Spectral transmittance improved by about 1.5 times from 60% (pristine) to 90% (treated). An interplay between the roughening action of ion etching and the smoothing action of surface diffusion serves as the physical basis for the formation of sharp-tipped, tapered nanostructures on the lens surfaces. The introduction of nanostructures on the surface effectively created a hydrophobic, antireflective interface. Pre- and post-treatment FTIR-ATR transmittance peaks remained unaltered. Hence surface changes are attributed to physical factors and not to any chemical reactions.

Key Words

CR-39; Nanostructures; Ion source; FTIR-ATR; AFM; Spectral transmittance.

INTRODUCTION

Surface modification or surface engineering has long since been employed as a method for improving the performance of materials. The technology has grown considerably in the past few decades having been proven that significant gains in performance and economic advantages can be attained by simply altering the physicochemical characteristics of the surface from that of the bulk material^[1]. Plasma assisted surface modifications are of special inter-

est since these have applications in commercial treatment of materials in a sterile environment, without the use of potentially harmful chemicals^[2-3]. According to the physical model proposed by Bradley and Harper (BH theory), ion bombardment acts as a driving force to roughen the surface by random removal of atoms while surface diffusion acts to restore the surface to a flat equilibrium state. The balance between roughening due to sputtering and various smoothing mechanisms can lead to a wide range of morphologies^[4,5]. That is why different substrates pro-

cessed at different experimental parameters would yield differences in physical, chemical and optical properties.

This study attempts to investigate the influence of Low Energy Hydrogen Ion Shower (LEHIS) on the physico-chemical and optical properties of a known thermally and chemically stable, physically durable material such as Allyl Diglycol Carbonate polymer, where its usefulness lies largely on its optical properties. The material commercially referred to as CR-39 (patented and exclusively produced by PPG Industries Inc., CR for Columbia Resin), can be polymerized to produce cross-linked homopolymers or copolymer systems^[6]. CR-39 is used as a monomer to make thermoset plastics, where its principal uses include protective covers for welding lenses, safety shields and guards, laboratory equipment, radiation detection devices, photographic filters, and ophthalmic lenses. Plastic lenses made from CR-39 polymers are known for their chemical, thermal and mechanical resistance, coupled with optical properties comparable to that of glass. Thus, CR-39 ophthalmic lenses have become the most widely used material for eyewear lenses worldwide, becoming commonly referred to as “plastic” eyeglass lens. Previous studies aiming to enhance transmittance and other optical properties of CR-39 polymer either focused on thin film coatings^[7], or through modifications in the polymerization process. Little readily available literature can be found that discuss direct surface lens modification.

There are two ways in which CR-39 ophthalmic lens is manufactured. The first process is by mold polymerization wherein CR-39 in liquid form is injected and polymerized in a curved mold. The second process is by sequential thermal polymerization wherein CR-39 is polymerized in a large plane mold, cut into suitable sizes and undergoes hot deformation into the suitable shape. Due to the advantage of mass production, the latter is a cheaper method but produces lens of inferior quality because of mechanical stress during the fabrication process. A locally fabricated clear lens from this method gives an optical transmittance of about 60 % only. By nanotexturing the surfaces of these lenses via LEHIS irradiation, spectral transmittance was enhanced to 90% level.

MATERIALS AND METHODS

Plasma facility and the CR-39 substrates

Figure 1(a) shows the CR-39 ophthalmic lenses used in this work. Each substrate lens measured $6 \times 6 \times 2 \text{ mm}^3$. These were irradiated with H_n^+ ions from a Gas Discharge Ion Source (GDIS). Figure 1(b) shows the schematic diagram of the overall facility and Figure 1(c) presents a 3D figure of the GDIS. It has a compact discharge region of volume 0.8 cm^3 and an exit aperture of 2.0 mm in diameter. The extraction and focusing electrodes were grounded to ensure a diffused ion shower

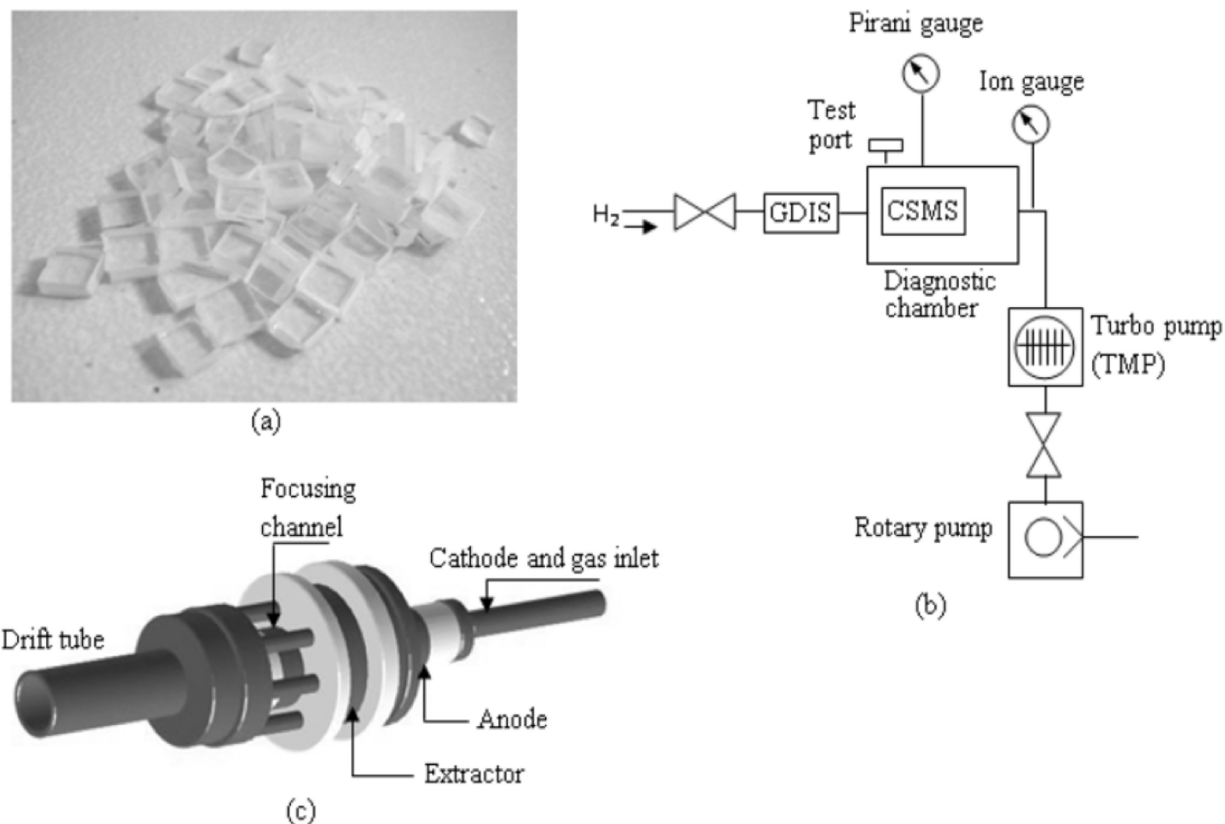


Figure 1 : (a) CR-39 ophthalmic lenses used in the study. (b) schematic diagram of the overall facility. (c) 3-D figure of the compact Gas Discharge Ion Source.

configuration. The GDIS fits a standard 70 mm knife-edge flange coupled to a plasma reactor whose volume is about 2400 cm³. The system is pressure regulated by a 50 l/s turbo molecular pump backed up by a 16 m³/h rotary pump. Complete details of the facility are described in earlier reports^{18,91}.

Beam characterization

Prior to the treatment process, beam diagnostics were done using (i) a Cast Steel Mass Spectrometer (CSMS) to identify the ion species and measure their respective current densities in the beam and (ii) a Single Slit Multi-Detector (SSMD) emittance meter to measure beam emittance. The design and operational characteristics of the CSMS have been reported in an earlier article¹⁰¹. The schematic and 3-D illustration of the SSMD meter is shown in Figure 2. It consists of a stainless steel casing with dimensions 23 mm x 23 mm x 123 mm. At the front end is a slit measuring 0.5 mm in width and 12 mm in length. Fifteen sheets of thin metal plates each 0.3 mm thick, 25 mm

long and 10 mm wide, are mounted on the rear end of the device. These plates function as current detectors. A Mylar sheet 0.05 mm thick is inserted between adjacent detectors for insulation. Hence, there is a stack-wise arrangement of stainless steel and Mylar sheets in the direction parallel to the beam axis. Distance between slit and detector stack is 90 mm. The detectors in turn are electrically coupled to a multiplexer-electrometer circuit that simultaneously measures the ion signals detected. Automatic data acquisition and processing routines were employed by both CSMS and SSMD. Raw signals detected by the CSMS were converted into ion peaks. Beamlet intensity profiles traced by the SSMD were converted into two-dimensional phase-space projections of the beam volume, commonly known as emittance contours. Emittance (ϵ) provides a quantitative basis, or a *figure of merit*, for describing the quality of a charged particle beam. It is a two-dimensional projection of the volume occupied by the ensemble of particles in six dimensional phase space defined by spatial and momentum coordinates¹¹¹.

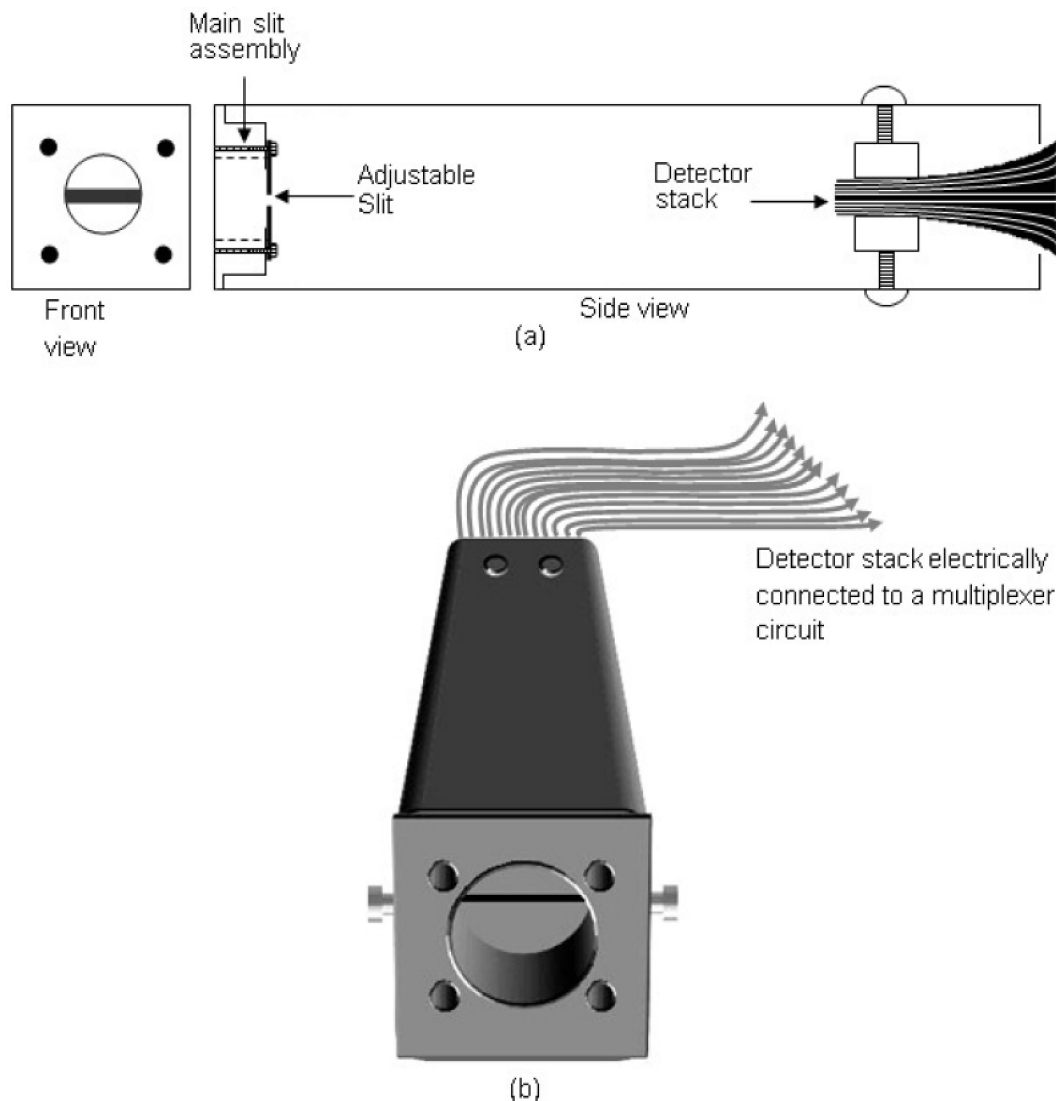


Figure 2 : (a) Schematic diagram of the single slit multi-detector (SSMD) emittance meter. (b) 3-D diagram of the SSMD.

Treatment process

The pressures inside the reactor chamber were monitored using Pirani and ionization gauges. The facility was evacuated up to a base pressure of 1.0×10^{-6} Torr. Hydrogen gas feed was varied from 3 to 5 mTorr depending on the dose of the constituent ions needed. The CR-39 samples were positioned 70 mm downstream measured from the beam portal. Processing time was maintained at 15 minutes for each sample.

Sample characterization

Four characterization tests were performed on the CR-39 samples. 1) Atomic Force Microscopy (AFM) to extract surface topographical information using the Solver PRO-M model Scanning Probe Microscope, 2) Fourier Transform Infrared with Attenuated Total Reflectance (FTIR-ATR) spectroscopy to identify changes in the chemical constituents of the substrate lenses using the SHIMADZU IR Prestige21 FTIR Spectrometer, 3) Spectral transmittance measurements by means of the SHIMADZU UV-3700 UV-VIS-NIR Spectrophotometer, to determine the fraction of incident light that passed through the lenses and 4) Wettability test or the sessile drop contact angle measurement to determine the water sorption attributes of the samples.

Details and limitation of the wettability test

In the wettability test, contact angle (CA) is defined as the angle between the droplet baseline and the tangent to the drop-shape. The test was performed making use of the Intel 1 Play TM QX3TM Computer Microscope. A 1 μ L droplet of distilled deionized water was placed above the substrate surface using a micro-syringe. Images of the water droplets were recorded sequentially at different sites. Data was considered acceptable only if the CA, after three repetitions differed by not more than 10%. Hence, each contact angle is actually a mean value, averaged over three different points on the sample. Contact angles were measured digitally using Scilab, an open-source image-processing program. In this work only *static contact angle* was exploited as the direct parameter to wettability. At this juncture of the research, focus is on surface energetics in static equilibrium. Hence data on the phenomenon of hysteresis involving advancing and receding contact angles were ignored- as of now. All information about the wettability (more importantly the hydrophobicity) of the surface was interpreted from static contact angle data.

RESULTS AND DISCUSSION

AFM results vis-à-vis ion shower characteristics

Figures 3(a), (b), (c) and (d) are representative AFM

images of the control, 1mA, 2 mA and 5 mA treated samples respectively. A distinct contrast can be seen between the pristine (i.e., control) and treated samples. The former shows an irregular surface with craters of diverse shapes whereas the processed samples show a much smoother exterior in that the depressions are no longer visible. The treatment has grown a layer of nano-sized structures exhibiting a more even exterior. Mass spectrometry (Figure 5) shows LEHIS irradiation with ion ratios of $H^+/H_2^+ > 8$ produced this ubiquitous feature of nanostructures on the surfaces. Such nanotexturing action is the result of an interplay between ion bombardment which serves to roughen the surface by random removal of atoms, and surface diffusion which acts to equilibrate the surface through adatom diffusion^[12]. However at higher discharge conditions, i.e., discharge currents ($I_d > 3$ mA), discharge voltage ($V_d > 1$ kV) where $H^+/H_2^+ < 8$, hardly any nanostructures were formed on the surface.

Figures 4 (a), (b) and (c) are AFM histograms showing typical average surface roughness of the pristine and treated samples. Surface roughness decreased from 30.91 nm for the pristine sample to 12.94 nm for the LEHIS treated sample where V_d was maintained below 1 kV, $I_d = 1$ mA, $H^+/H_2^+ > 8$. At high discharge showers ($I_d = 5$ mA, $V_d = 3.5$ kV), with high doses of H_2^+ , the etching effects of these more massive diatomic ions effaced the nanostructures that may have been formed, increasing average surface roughness to 20.33 nm shown in Figure 4(c).

Figure 5 shows the ion shower mass spectra captured by the CSMS. Current densities provide a representative measure of the bombarding energies of ions. The current density of H_2^+ is much higher at 5 mA discharge causing surface degradation thus the increase in surface roughness. It is plausible that high energy H_2^+ ions inhibited the formation of nanostructures.

Interestingly, the emittance contour of the 5 mA discharge shows greater distortion compared to the approximately elliptical-shaped contours of LEHIS, seen in Figures 6(a), (b) and (c). It would appear that a distorted, larger emittance contour is associated to a highly abrasive ion shower that promotes surface erosion not conducive to nanotexturing. The increase in emittance may be due to collisions between beam particles, i.e., Coulomb scattering between different hydrogen ion species^[11]. Here, it is believed that the ion shower loses its laminar flow causing particles to approach the substrate anisotropically, thus displaying abrasive etching.

FTIR results

FTIR-ATR characterization was conducted to determine whether or not the bombarding hydrogen ions had any effect on the chemical structure of the samples. The treated samples exhibited signature peaks of CR-

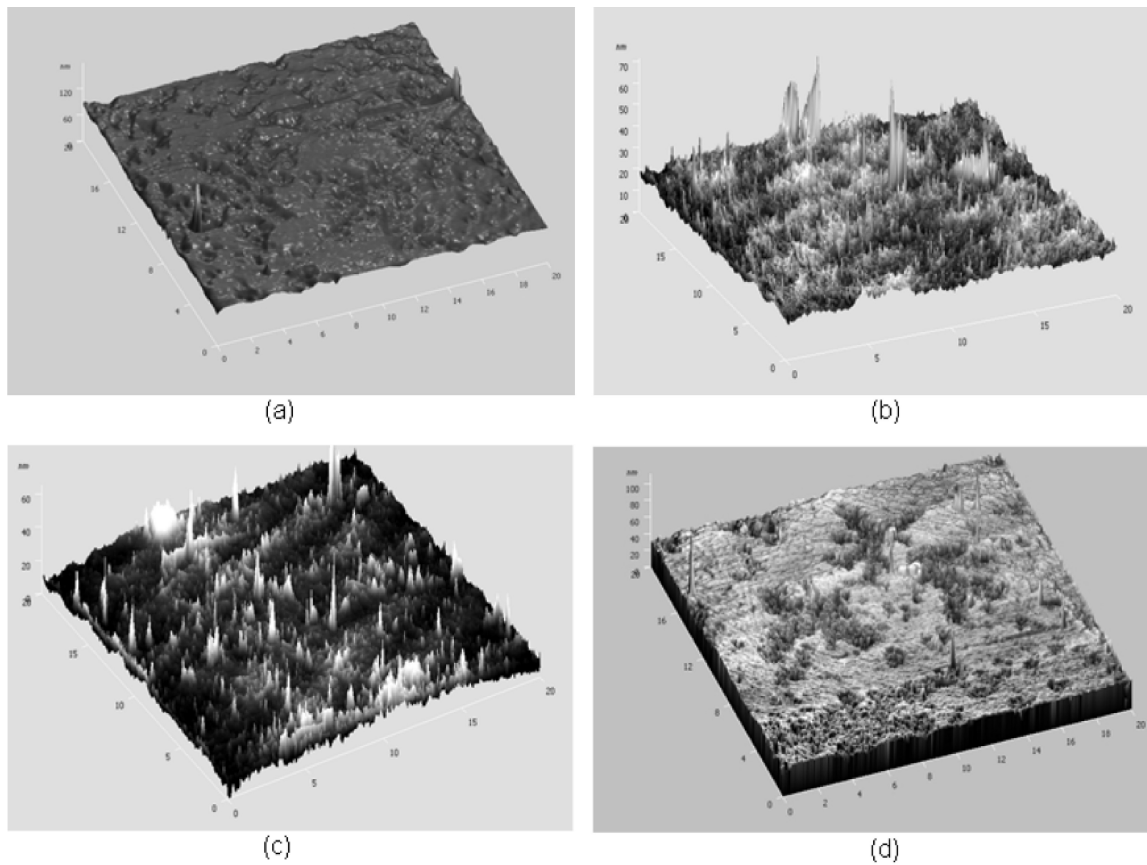


Figure 3 : AFM image of (a) untreated sample (control), (b) sample irradiated by 1 mA discharge hydrogen ion shower (c) sample irradiated by 2 mA discharge ion shower, (d) sample irradiated by 5 mA discharge ion shower.

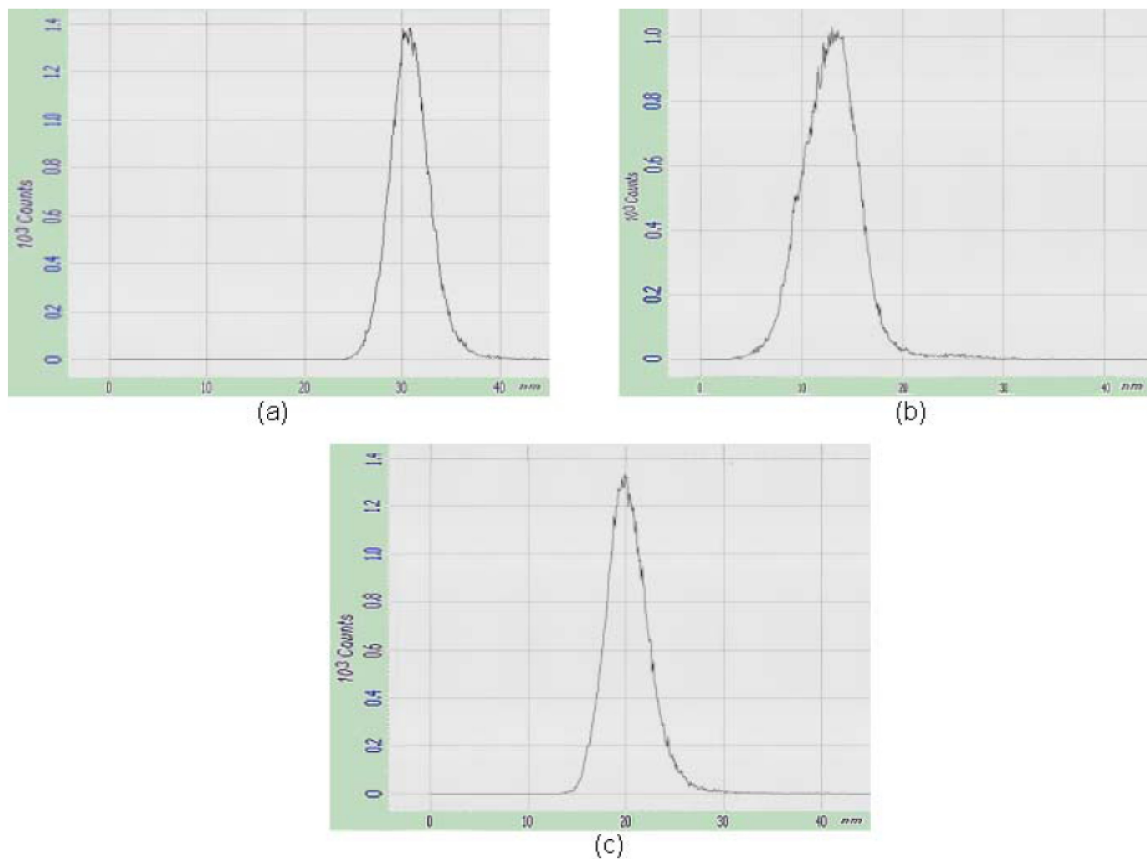


Figure 4 : AFM histograms showing typical average surface roughness of (a) pristine sample, (b) LEHIS treated sample ($I_d \leq 3$ mA, $V_d \leq 1.5$ kV) and (c) sample treated with high energy ion shower ($I_d > 3$ mA, $V_d > 1$ kV).

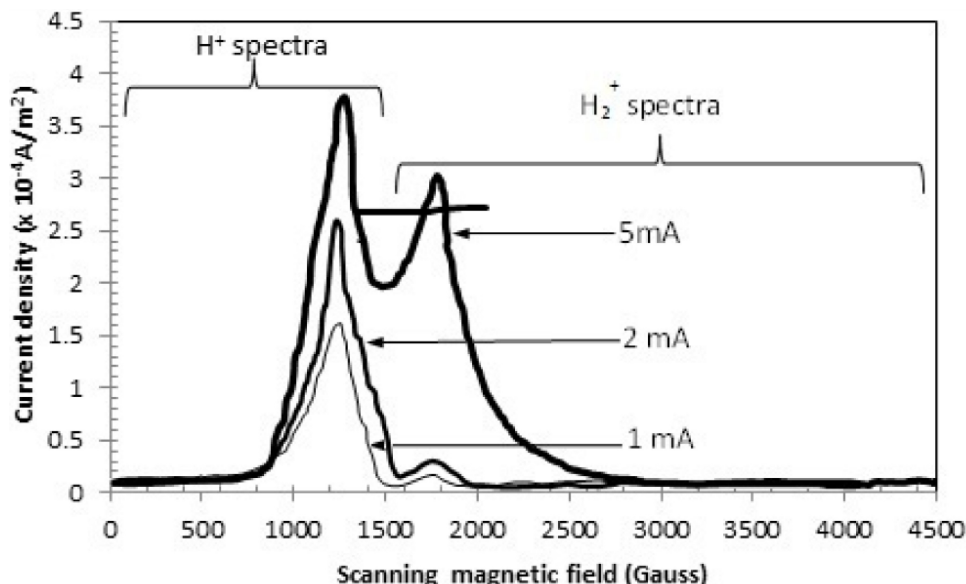


Figure 5 : Mass spectra of the hydrogen ion showers used in the irradiation process. Ion ratio of LEHIS ($I_d = 1$ to 3 mA, $V_d < 1$ kV) is $H^+/H_2^+ > 8$, while that of high discharge showers ($I_d > 3$ mA, $V_d > 1$ kV) is $H^+/H_2^+ < 8$.

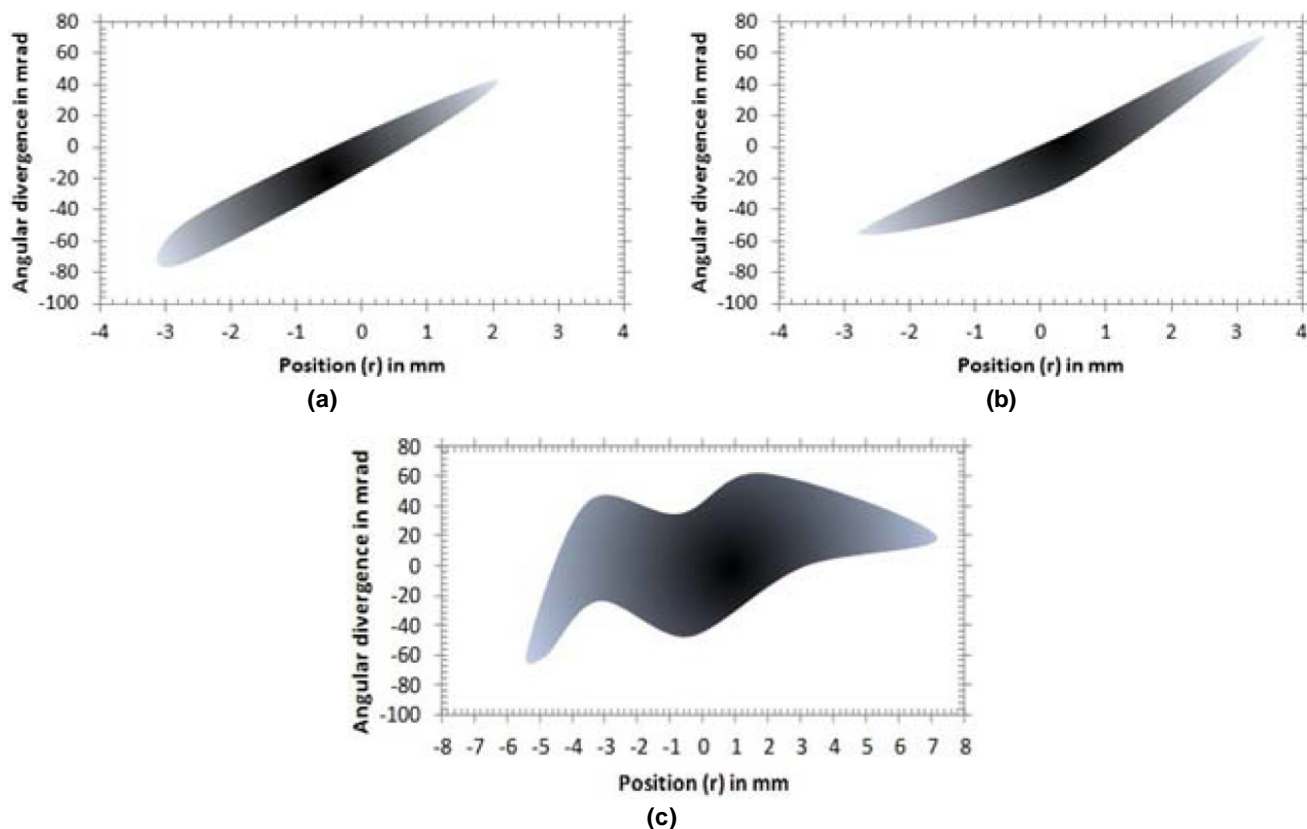


Figure 6 : Emittance (ϵ) contours of the H_n^+ ion showers plotted at 90 % beam fraction for: (a) 1 mA discharge, $\epsilon = 180$ mm-mrad, (b) 2 mA discharge, $\epsilon = 195$ mm-mrad, and (c) 5 mA discharge, $\epsilon = 310$ mm-mrad. High discharge treatment currents show highly distorted emittance contours.

39. Shown in Figure 7, the peaks corresponding to C=O stretching vibration (1766 , 1264 and 1141 cm^{-1}), C–O–C stretching vibration (1096 and 1026 cm^{-1}), –CH=CH₂ stretching vibration (3074 and 1650 cm^{-1}), C=C deformation vibration (964 cm^{-1}), C–H stretching vibration (2952 cm^{-1}), C–H deformation vibration (1456 , 1405 , 879 and 788 cm^{-1}) observed in the treated samples are

all characteristics of CR-39 polymers^[13,14]. The only change that may be indicative of a chemical change is the slight shortening of the C–H stretching vibration peak at 2952 cm^{-1} , which belongs to asymmetric CH₂ stretching vibrations for aliphatic hydrocarbons. This may simply be due to a deformation of the bonds caused by surface heating during treatment. For lack of any significant

change in the transmittance peaks, the chemical compositions remain basically unaltered. Surface changes can only be attributed thus far to physical factors and not to any chemical reactions.

Wettability test vis-à-vis ion shower characteristics

Contact angle of the samples versus ion density ratio and discharge voltage are reported in Figure 8. The contact angle is observed to decrease at increasing discharge voltage and H_2^+ fluence. LEHIS irradiation ($I_d = 1$ to 3 mA, $V_d < 1$ kV) produced nanotextured surfaces inducing high CA of up to 123° . The presence of nanometer sized

asperities minimized the surface free energy inducing hydrophobicity.

Surfaces bombarded by higher discharges ($I_d > 3$ mA, $V_d > 1$ kV) on the other hand exhibited sparse growth of the surface nanostructures as shown in the flat data reconstruction of Figure 9. Hence, water repellent lenses can be produced provided the proper chemical feature of the ion shower is imparted on the surface. An ion shower with H^+ to H_2^+ ratio of 8 or greater ($H^+/H_2^+ \geq 8$) sculpted hydrophobic surfaces densely packed with nanostructures. Below this ratio, the ion showers became highly energetic and abrasive, inimical to nanotexturing.

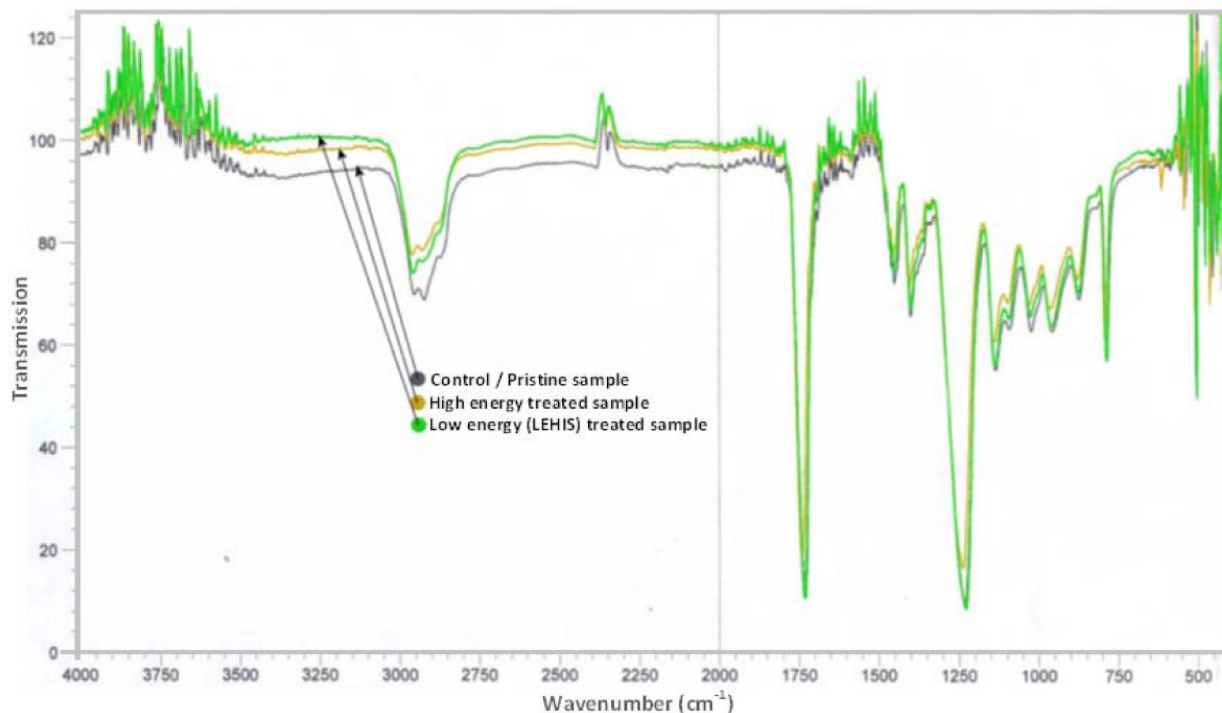


Figure 7 : FTIR spectra of the pristine and treated CR-39 ophthalmic lenses.

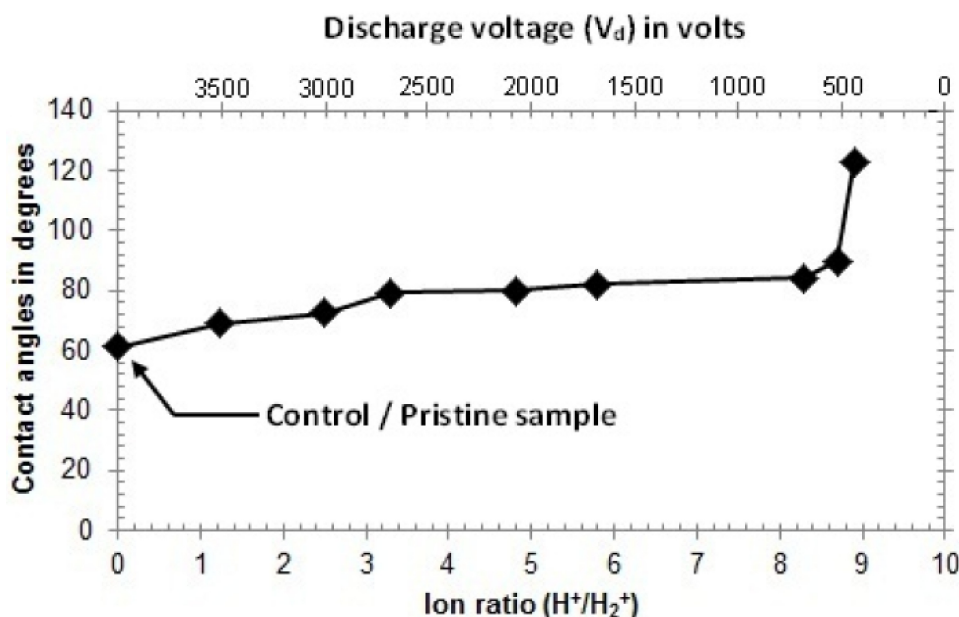


Figure 8 : Contact angle of the samples versus ion density ratio (H^+/H_2^+) and discharge voltage (V_d).

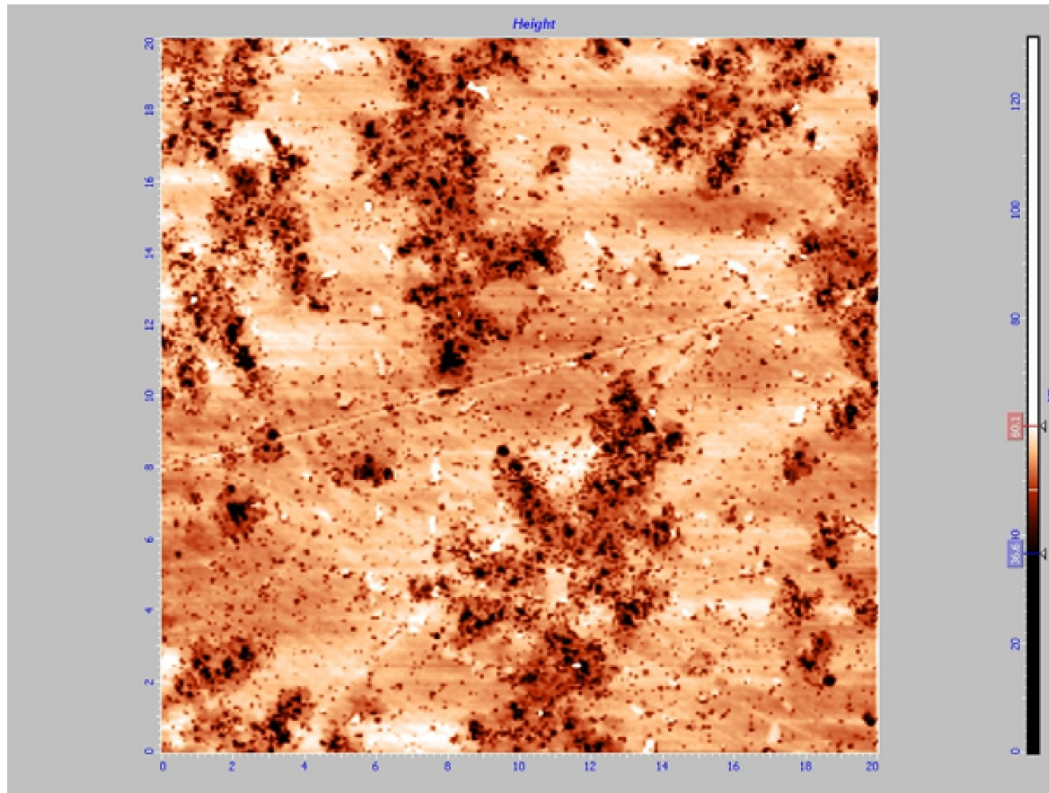


Figure 9 : Typical flattened data reconstructions of surfaces treated with high energy showers.

Spectral transmittance vis-à-vis ion shower characteristics

The spectral transmittance measurements are shown in Figure 10. LEHIS treated samples transmitted significantly more light than the control. Results showed an average increase of 50% from a low of 61% transmittance for the control to a high of 91% transmittance for the 1mA treated sample.

Introducing fine irregularities on the surface (physical etching) has been known to effectively create an antireflective interface for some polymers due to a refractive index gradient^[15]. The formation of nanometer sized, tapered-structures commonly known as Sub-Wavelength Structures (SWS), enhanced the refractive index gradient which refracted light into the bulk material resulting in diminished reflection and improved transmission. A pertinent feature of SWS is its tapered physical configuration that matches the optical impedance of two adjacent media at their interface, minimizing reflection and improving photon collection efficiency^[16]. This particular functionality is achieved in insects e.g, butterflies and moths, by an array of tapered elements in their eyes allowing them to see under low-light conditions^[17-20]. There are currently two existing theories that explain the refractive index gradient phenomenon. The first, known as the effective medium theory^[21], describes the effective dielectric constant of homogeneously mixed materials. As the fraction of air around these tapered structures progressively decrease

from the top of the tip to its base, the refractive index correspondingly changes. Meaning, incident light propagates through the surface as if it is going through a gradient index environment, thus rendering low reflectance^[22]. Another proposed theory is the similarity of moth eye microstructures to sub-wavelength diffraction gratings. Diffraction theory states that when the period of the grating is smaller than the wavelength of incident light, reflective diffraction is minimized^[23]. Numerical simulations^[24] revealed that high aspect ratio gratings of tapered structures like nanotips exhibit reflectance much smaller than pillar-like nanostructures. The key to this effect is the difference in physical size from the tip of the structure to its base. Meaning, the crucial factor that minimizes reflection and thus increases transmission is the non-uniform distribution of air across the structure. Samples that were irradiated with high energy showers showed lower average transmittance compared to the LEHIS treated samples. The 4 mA treated sample measured an average of 78 % transmittance while the 5 mA sample measured 73 %. This is attributed to a lower population density of nanostructures on their surfaces. With less tapered nanostructures to provide the refractive index gradient, the efficiency of the surface to suppress reflection suffered, thus reducing transmittance.

The presence of nanostructures is essentially the reason for the reduction of light reflectance (moth-eye effect) of transparent polymers. Blending polymer material with air on a sub-wavelength scale reduces the refractive

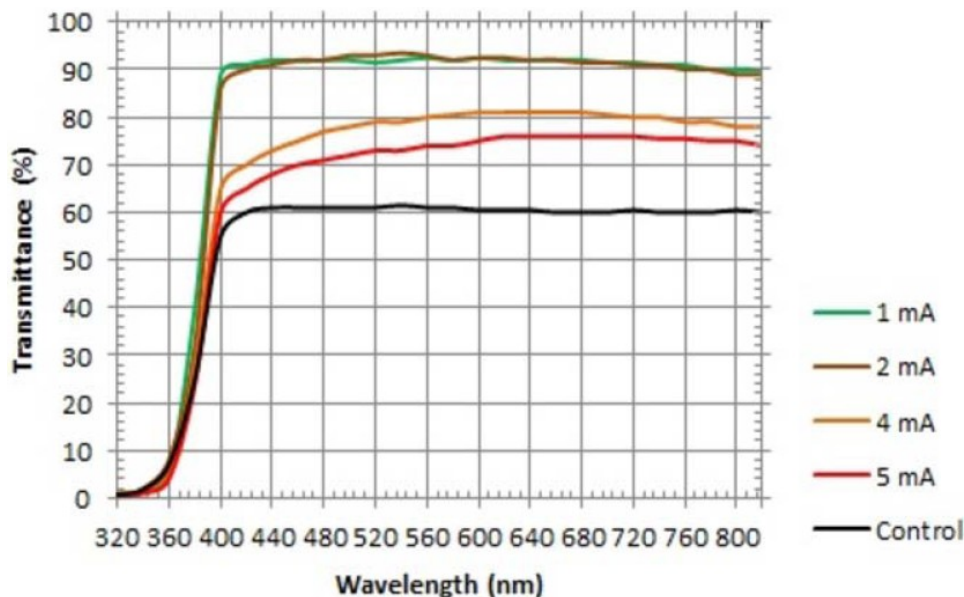


Figure 10 : Spectral transmittance profile of the samples as a function of discharge current (I_d).

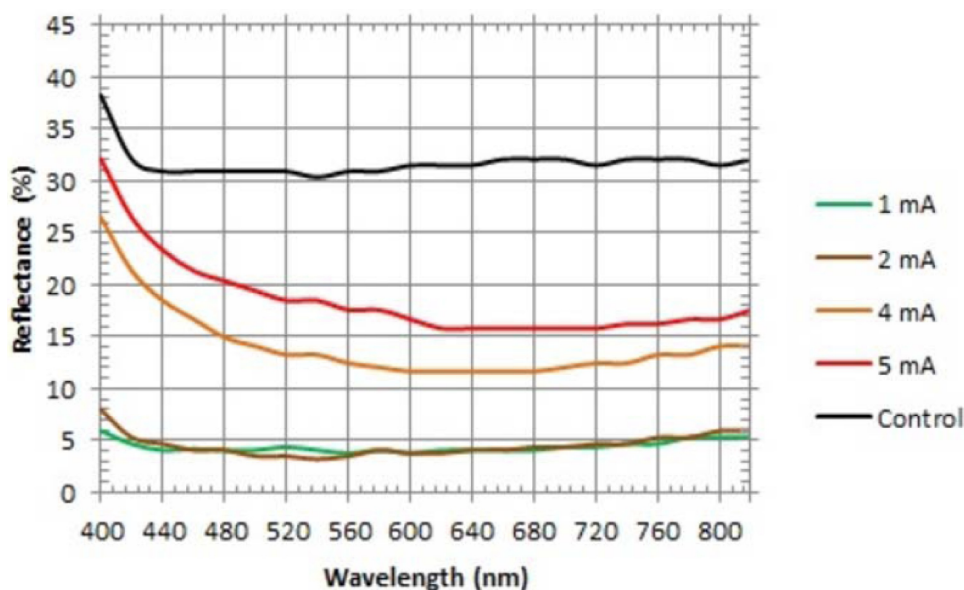


Figure 11 : Reflectance profile of the samples as a function of discharge current (I_d).

index, thereby reducing reflectance^[25]. Figure 11 shows the reflectance measurements of the samples. The LEHIS treated lenses showed minimal mean reflectance of 4.5 % as opposed to 14 to 19 % for the high energy treated samples and 32 % for the control.

CONCLUSION

The interplay between ion roughening (LEHIS irradiation) and surface diffusion induced the formation of fine, sharp-tipped, tapered irregularities on the surface of CR-39 ophthalmic lenses. LEHIS treatment effectively: (i) suppressed Fresnel reflectance which resulted in higher transmittance by about 1.5X from 61% to 91% and (ii) enhanced the degree of hydrophobicity with contact angles increasing from 61.23° to 122.64°. The

tapered structure ensured a refractive index gradient for antireflection, and the sharp tip minimized contact area in the liquid-solid interface which favored enhanced hydrophobicity. There appears to be a causal relation between ion shower characteristics and nanotexturing. The most apparent correlation is the requirement of H^+ to H_2^+ ratio of 8 or greater ($H^+/H_2^+ \geq 8$) which favors nanohill formation. The correlation between the physical configuration of beam emittance and surface topographic relief is also strong. The more distorted the emittance contour, the rougher the treated surface becomes macroscopically, and the less likely nanostructures will be formed. FTIR-ATR results show minimal changes in the chemical make-up of the lenses, pre- and post LEHIS treatment. Hence the surface modification process is purely physical.

REFERENCES

- [1] W.A.Bryant; Surface Modification Engineering, R.Kossowsky, (Ed); CRC Press Inc., Boca Raton, Florida, **1**, (1989).
- [2] G.Q.Blantocas, A.S.Al-Aboodi; Physicochemically modifying wood by low energy hydrogen ion shower: An alternative plasma-based antitermite method, *Wood.Fiber Sci.*, **43(4)**, 449-456 (2011).
- [3] H.S.Salapare III, G.Q.Blantocas, V.R.Noguera, H.J.Ramos; Low-energy hydrogen ion shower (LEHIS) treatment of polytetrafluoroethylene (PTFE) materials, *Appl.Surf.Sci.*, **255**, 2951-2957 (2008).
- [4] U.Schulz, P.Munzert, R.Leitel, I.Wendling, N.Kaiser, A.Tünnermann; Antireflection of transparent polymers by advanced plasma etching procedures, *Opt.Express.*, **15(20)**, 13108-13113 (2007).
- [5] R.M.Bradley, J.M.Harper; Theory of ripple topography induced by ion bombardment, *J.Vac.Sci.Technol.A*, **6**, 2390-2395 (1988).
- [6] PPG Industries, Inc.; CR-39 Product Bulletin, <http://www.trinitylens.com/CR39.pdf>; (Accessed 18 March 2014), (2006).
- [7] M.C.Coen, R.Lehmann, P.Groening, L.Schlapbach; Modification of the micro- and nanotopography of several polymers by plasma treatments, *Appl.Surf.Sci.*, **207**, 276-286 (2003).
- [8] G.Q.Blantocas, P.E.R.Mateum, R.W.M.Orille, R.J.U.Ramos, J.L.C.Monasterial, H.J.Ramos, L.M.T.Bo-ot; Inhibited flammability and surface inactivation of wood irradiated by low energy hydrogen ion showers, *Nucl.Instrum.Meth.*, **B259**, 875-883 (2007).
- [9] G.Q.Blantocas, H.J.Ramos, M.Wada; Surface modification of narra wood (*Pterocarpus Indicus*) by ion shower treatment, *Jpn.J.Appl.Phys.*, **45**, 8525-8530 (2006).
- [10] G.Q.Blantocas, H.J.Ramos, M.Wada; Design and operational characteristics of a cast steel mass spectrometer, *Rev.Sci.Instrum.*, **75**, 2848-2853 (2004).
- [11] M.Reiser; Theory and Design of Charged Particle Beams, John Wiley & Sons, Inc., New York, (1994).
- [12] R.Di Mundo, V.De Benedictis, F.Palumbo, R.d' Agostino; Fluorocarbon plasmas for nanotexturing of polymers: A route to water-repellent antireflective surfaces, *Appl.Surf.Sci.*, **255**, 5461-5465 (2009).
- [13] K.C.C.Tse, D.Nikezic, K.N.Yu; Comparative studies of etching mechanisms of CR-39 in NaOH/H₂O and NaOH/ethanol, *Nucl.Instrum.Meth.*, **B263**, 300-305 (2007).
- [14] H.A.Al-Jobouri, N.R.Jber, A.H.Al-Shukrawi, M.K.Hamid; Physicochemical properties of crystalline etch products for CR-39 trackdetector after α -particles irradiation, *Adv.Appl.Sci.Res.*, **4(4)**, 501-507 (2013).
- [15] A.Kaless, U.Schulz, P.Munzert, N.Kaiser; NANO-motheye antireflection pattern by plasma treatment of polymers, *Surf.Coat.Technol.*, **200**, 58-61 (2005).
- [16] S.Chattopadhyay, Y.F.Huang, Y.J.Jen, A.Ganguly, K.H.Chen, L.C.Chen; Anti-reflecting and photonic nanostructures, *Mater.Sci.Eng.R*, **69**, 1-35 (2010).
- [17] S.J.Wilson, M.C.Hutley; The optical properties of 'Moth Eye' antireflection surfaces, *Opt.Acta*, **29**, 993-1009 (1982).
- [18] D.G.Stavenga, S.Foletti, G.Palasantzas, K.Arikawa; Light on the moth eye corneal nipple array of butterflies, *Proc.Roy.Soc.B*, **273**, 661-667 (2006).
- [19] A.R.Parker, Z.Hegeudus, R.A.Watts; Solar-absorber antireflector on the eye of an Eocene fly (45 Ma), *Proc.R.Soc.B*, **265**, 811-815 (1998).
- [20] A.R.Parker, H.E.Townley; Biomimetics of photonic nanostructures, *Nat.Nanotech.*, **2**, 347-353 (2007).
- [21] G.Vasan; Numerical Investigation of Rough Model Surfaces in Attenuated Total reflection Surface Enhanced Infrared Absorption Spectroscopy with Correlating Experiments. Ph.D. Dissertation, Faculty of Mechanical Engineering Ruhr University Bochum, (2012).
- [22] P.Clapham, M.Hutley; Reduction of lens reflexion by the "Moth Eye" principle, *Nature*, **244(5414)**, 281-282 (1973).
- [23] H.L.Chen, S.Y.Chuang, C.H.Lin, Y.H.Lin; Using colloidal lithography to fabricate and optimize sub-wavelength pyramidal and honeycomb structures in solar cells, *Opt.Express*, **15(22)**, 14793-14803 (2007).
- [24] Y.M.Song, H.J.Choi, J.S.Yu, Y.T.Lee; Design of highly transparent glasses with broadband antireflective subwavelength structures, *Opt.Express*, **18(12)**, 13063-13071 (2010).
- [25] A.Gombert, W.Glaubitt, K.Rose, J.Dreibholz, B.Bläsi, A.Heinzel, D.Sporn, W.Döll, V.Wittwer; Subwavelength-structured antireflective surfaces on glass, *Thin Solid Films*, **351**, 73-78 (1999).